Batteries & Supercaps

Research Article
doi.org/10.1002/batt.202500320

Chemistry Europe
European Chemical Societies Publishing

www.batteries-supercaps.org

Thermally Stable $LiNi_{0.6}Mn_{0.15}Co_{0.15}Al_{0.05}Ti_{0.05}O_2$ Layered Cathode for Lithium-Ion Batteries: Experimental and Theoretical Study

Vasantha A. Gangadharappa, Pandiarajan Devi, Vinoth Kumar Jayaraman, Anil Kumar U, Palanichamy Murugan, and Annigere S. Prakash*

Lithium-ion batteries (LIBs) have gained widespread adoption in the automotive and smart electronics industries. However, there are growing public concerns regarding the potential risk of thermal runaway incidents, which can be triggered by internal short circuits, overcharging, or physical damage. To ensure the safety of battery systems and minimize the risk of thermal runaway, it is essential to prioritize design, safety protocols, and material selection. The choice of cathode material is particularly significant in mitigating this risk. In response to this challenge, a thermally stable cathode material called $LiNi_{0.6}Mn_{0.15}Co_{0.15}Al_{0.05}Ti_{0.05}O_2$ (NMCAT) has been formulated here and its structural, morphological, electrochemical, and thermal characteristics are investigated. The thermal and electrochemical characteristics of NMCAT have revealed promising findings. The incorporation of aluminum (Al) and titanium (Ti) in the cathode formulation has resulted in improved thermal stability, enabling the material to withstand temperatures up to 280 °C without compromising its capacity. Further, a detailed atomic-level understanding of the thermal stability has been revealed through first-principles calculations, which complement the experimental data. This breakthrough in enhancing thermal stability is essential for mitigating the risks associated with thermal runaway in LIBs from a material perspective.

1. Introduction

Lithium-ion batteries (LIBs) have experienced rapid growth in various sectors, including portable electronics, power tools, electric vehicles, commercial buildings, and electrical grids.[1] This is primarily due to their desirable features such as high energy density, low self-discharge, absence of memory effect, and wide voltage operating range.[2] However, alongside these attractive attributes, thermal runaway poses a significant safety concern for LIBs, as they are sensitive to temperature variations.

Thermal runaway in LIBs is typically triggered by three types of abuses: mechanical, electrical, and thermal. Mechanical abuses include accidents, crashes, nail penetrations, or damage to the battery casing. Electrical abuses can result from overcharging or inadequate battery management systems. Thermal abuses involve thermal shocks or insufficient cooling systems.[3,4]

Under these abusive conditions, heat can be generated through interactive reactions between the battery cell components or the decomposition of individual cell components.

According to Ying Sun et al., a potential sequence of exothermic reactions occurs inside LIBs,[5] ultimately leading to thermal runaway. The sequence unfolds as follows: 1) decomposition of the solid electrolyte interphase at the anode, which typically occurs at temperatures ranging from 80 to 90 °C; 2) reaction between the lithiated anode and the electrolyte; 3) decomposition of cathode materials at elevated temperatures, resulting in the release of O_2; and 4) reaction between the released O_2, lithiated anode, and the flammable electrolyte.

These chain reactions generate a significant amount of heat and release flammable and toxic gases such as (CO_2, CO, H_2, CH_4, C_2H_4, and C_2H_6).[6] This exothermic process contributes to the thermal instability of LIBs. As a result, ensuring the thermal stability of battery materials has become an urgent requirement for the battery industry. It calls for the development of innovative battery chemistries to enhance safety measures and mitigate the risks associated with thermal runaway in LIBs.

Considering this, the objective of the current research is to develop a thermally stable cathode material for LIBs. Among various cathode materials, $LiNi_xMn_yCo_zO_2$ compositions (where $x + y + z = 1$) have shown promise for LIBs due to their high theoretical capacity (greater than 200 mAh g^{-1}).[7] Extensive investigations have been conducted to improve the capacity, cycle life, cycle rate, and retention of $LiNi_xMn_yCo_zO_2$ materials.[8–11] However, there are limited studies available in the literature regarding their thermal characteristics. For instance, Nguyen et al. reported on the thermal stabilities of 18 650 cells containing cathode compositions

V. A. Gangadharappa, V. K. Jayaraman, A. K. U, A. S. Prakash
Council of Scientific and Industrial Research
Central Electrochemical Research Institute-Chennai Unit, CSIR Madras Complex
Taramani, Chennai 600113, India
E-mail: prakash@cecri.res.in

V. A. Gangadharappa, P. Devi, A. K. U, P. Murugan, A. S. Prakash
Academy of Scientific and Innovative Research (AcSIR)
Ghaziabad 201002, India

P. Devi, P. Murugan
Electrochemical Power Sources Division
CSIR Central Electrochemical Research Institute
Karaikudi, Tamil Nadu 630003, India

Supporting information for this article is available on the WWW under https://doi.org/10.1002/batt.202500320

such as $Li(Ni_{0.8}Co_{0.15}Al_{0.05})O_2$ from Panasonic and $Li(Ni_{0.8}Mn_{0.1}Co_{0.1})O_2$ from LG.[12] Noh et al. indicated that Ni-rich ternary oxides offer higher energy density but lower thermal stability.[13] Feng et al. investigated the thermal stability of prismatic cells incorporating $LiNi_{0.4}Co_{0.4}Mn_{0.2}O_2$ through tests such as accelerating rate calorimetry (ARC) and differential scanning calorimetry (DSC).[14] Sun et al. explored the thermal runaway behavior of nickel-rich cathodes and found that $LiNi_{0.6}Co_{0.2}Mn_{0.2}O_2$ demonstrated greater stability compared to $LiNi_{0.8}Co_{0.1}Mn_{0.1}O_2$.[5] However, all these studies reported stability up to ≈250 °C. While numerous studies have focused on improving the performance and stability of $LiNi_xMn_yCo_2O_2$ cathode materials for LIBs,[15,16] there is a lack of comprehensive research on their thermal stability. Therefore, the aim of the present work is to further explore and enhance the thermal stability of cathode materials beyond the reported temperature range of 250 °C.

In this study, a Ni-rich cathode composition named "$LiNi_{0.6}Mn_{0.15}Co_{0.15}Al_{0.05}Ti_{0.05}O_2$" (NMCAT) is introduced, which exhibits thermal stability up to 280 °C. Thermodynamic analysis is conducted to gain insights into the reactions occurring within the layered metal-oxide cathodes during thermal runaway. Additionally, a comparison is made between the thermal characteristics of NMCAT and the commercially available pristine "$LiNi_{0.6}Mn_{0.2}Co_{0.2}O_2$" (NMC) cathode to provide a deeper understanding of their respective behaviors.

2. Experimental Section

The cathode material $LiNi_{0.6}Mn_{0.15}Co_{0.15}Al_{0.05}Ti_{0.05}O_2$ (NMCAT) was synthesized using the solution combustion method. To prepare the material, $LiNO_3$ (with an additional 10% to compensate during combustion and sintering losses), $Ni(NO_3)_2.6H_2O$, $Co(NO_3)_2.6H_2O$, $Mn(NO_3)_2.4H_2O$, $Al(NO_3)_3$, and $TiO(NO_3)_2$ were dissolved in distilled water, according the molar weight of each element in the formulation. Glycine (75%) and urea (25%) were added to the solution and mixed thoroughly. The complete solution was then transferred to an alumina crucible and placed in a preheated furnace at 750 °C (ramping at 5 °C min^{-1} holding at 1 h). The solution underwent boiling, leading to an exothermic reaction that ignited in less than 1 min. The crucible was removed from the furnace and allowed to cool down to room temperature. The resulting sample was ground for ≈15–20 min and subjected to sintering at normal air atmosphere 900 °C for 12 h (ramping at 5 °C min).

The structural parameters of the samples were obtained with diffraction patterns recorded using Bruker X-ray diffractometer D8 Advance model in the 2 Theta interval (10 to 70°). Rietveld refinements were performed using GSAS II tool. The crystal structures obtained through refinement were explored by the VESTA software.[17] The morphology of the powder samples was examined using a TESCAN Field Emission Scanning Electron Microscope (MIRA 3 model), at a magnification level of 15,000X. Electrochemical measurements were conducted using a VMPP3 battery cycler (plots are given in Supplementary Figure S2,S3,S4,S5, and S6, Supporting Information). Thermal stability characteristics were evaluated using a NETZSCH-STA 449F3 Thermogravimetric Analysis-DSC instrument by purging a nitrogen gas, with a heating rate of 1 °C per minute. The samples for DSC were prepared in an Ar filled glove box by crimping a cathode foil in an aluminum pan.

2.1. Structural and Morphological Characteristics

Figure 1a displays the X-ray diffraction patterns of the NMCAT material, which exhibit a good match with the ICDD PDF No (01-076-6561) database. The patterns are free from impurities and belong to the crystal space group R-3 m. Notably, the distinct splitting in the diffraction peaks at 65° indicate that the formed compounds are layered and well-ordered.[18] In addition, the diffraction patterns are fitted through Rietveld refinement. The R_w (5.53%), R_{bg} (5.84%), and Goodness of Fit index (1.2) values indicate that the results are reliable.

Figure 1b illustrates the corresponding crystal structure generated, revealing the arrangement of NMCAT as alternating Li slabs and metal oxide (Ni, Mn, Co, Al, or Ti) slabs. The Li and metal ions are octahedrally coordinated with oxygen, forming an ABCABC stacking pattern and resulting in a layered structure. The lattice parameters, specifically a, c, and volume, are determined to be 2.8697(5) Å, 14.2624(18) Å, and 101.72(1) $Å^3$, respectively. The 'a' parameter represents the distance between metal-metal intralayer distances, while the 'c' parameter denotes the combined thickness of the metallic layer and the LiO_6 layer.[19]

Figure 1c depicts the morphology of NMCAT, revealing the presence of a variety of structures of sizes ranging from 250 nm to 1 μm. The inset of Figure 1c, a magnified image (shown on the right), is composed of structures such as rhombohedral and hexagonal. The structural and morphological characteristics of commercial NMC622 are provided in the supplementary.

2.2. Thermal Characteristics

Thermal runaway in LIBs does not just happen when the battery is fully charged (states of charge (SOC)). It may happen at any SOC. Hence, we have chosen to examine the exothermicity at 50%, 75%, and 100% SOCs in this regard. As lithium is removed, the oxidation states of transition metals (especially Ni) increase, and the layered structure becomes metastable, prone to oxygen release. Materials such as Li_xNiO_2 and Li_xCoO_2 are known to evolve oxygen at elevated temperatures in their delithiated form, initiating exothermic decomposition reactions.[20] These reactions are closely associated with phase transitions,[21] notably from a layered structure to a spinel or rock-salt phase, which further accelerates degradation.

The thermal stability of NMCAT was investigated at different SOC, namely 100%, 75%, and 50%, as illustrated in **Figure 2**a. To assess the improved thermal stability of NMCAT, the results were compared with those of the commercially available pristine NMC622. At 100% SOC, NMCAT exhibited an exothermic peak at 281 °C with a ΔH value of 175.6 J g^{-1}, while the commercial NMC demonstrated exothermic behavior at 267 °C with a ΔH value of 353.8 J g^{-1}. Similarly, at 75% SOC, NMCAT displayed a peak at 280 °C with a ΔH value of 116.6 J g^{-1}, whereas the commercial NMC exhibited a peak at 267 °C with a ΔH value of

Research Article
doi.org/10.1002/batt.202500320
Chemistry Europe
European Chemical Societies Publishing

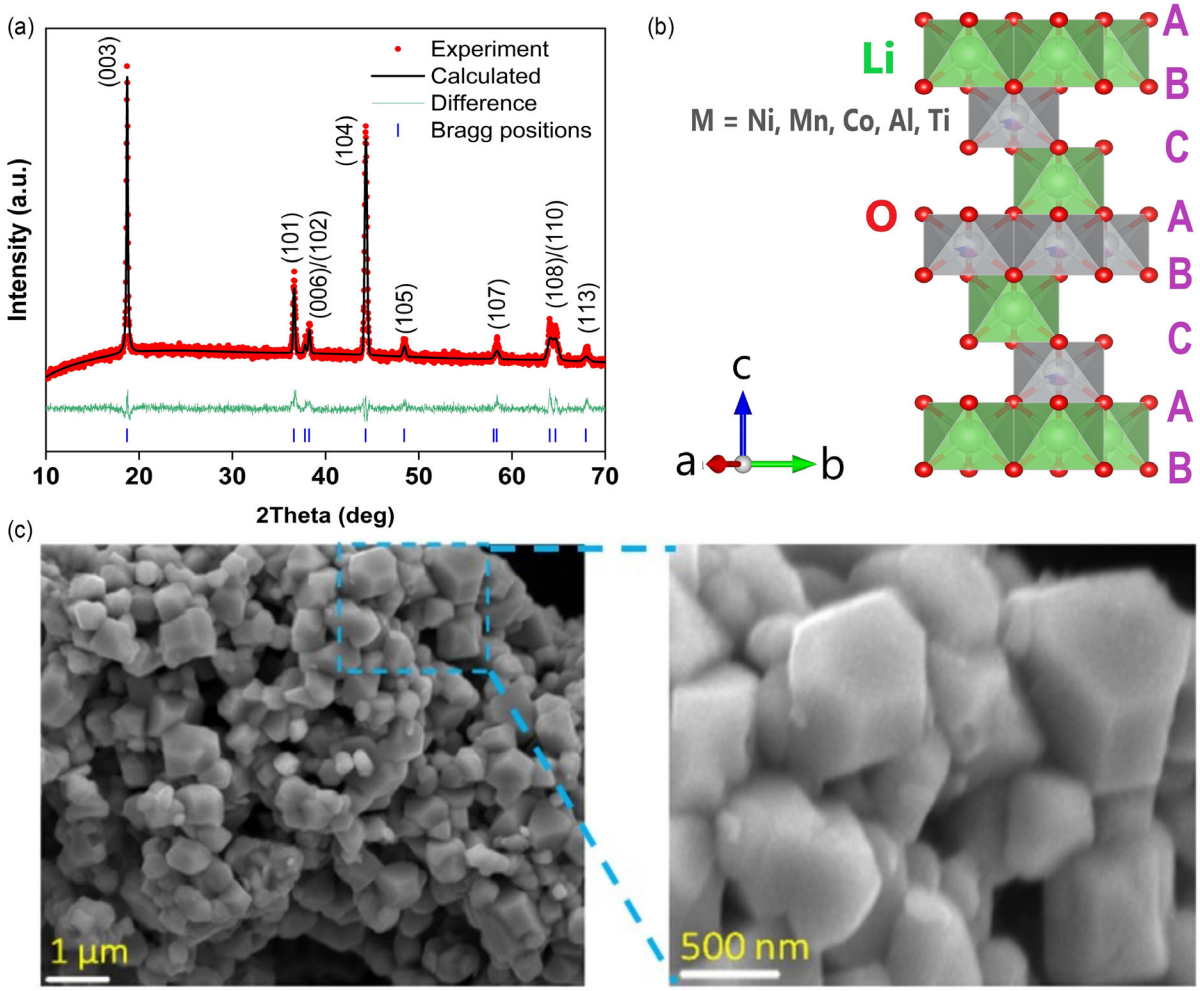

Figure 1. Structural and morphological characteristics of NMCAT. a) Rietveld's refinement of X-ray diffraction patterns of NMCAT, b) layered crystal structure of NMCAT generated from refinement, c) NMCAT morphology grabbed from field emission scanning electron microscopy with 11KX magnification, and the magnified image of the inset is shown on the right conformed of different shaped grains.

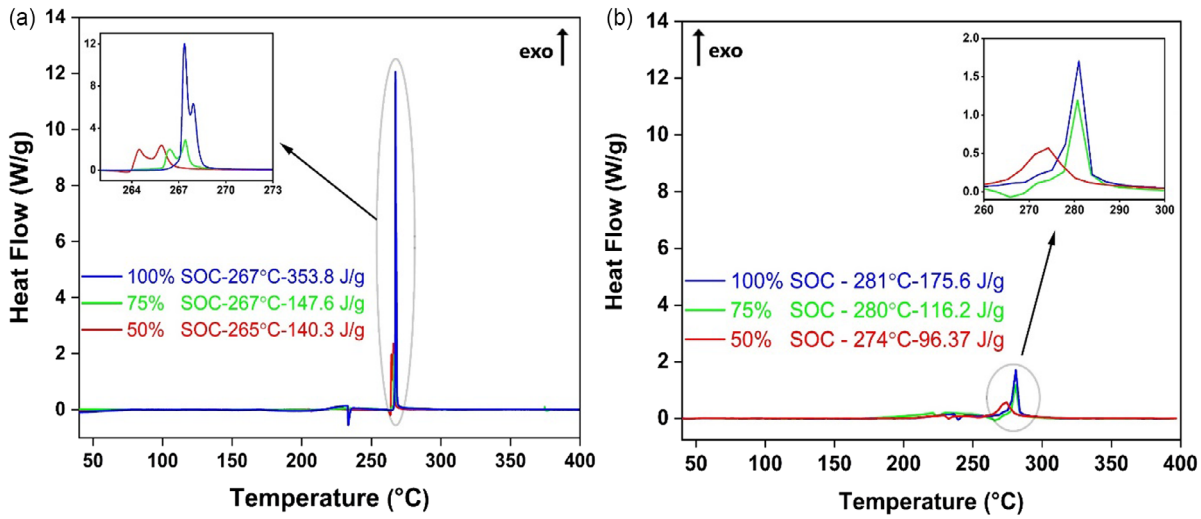

Figure 2. Comparison of DSC plots a) commercial $LiNi_{0.6}Mn_{0.2}Co_{0.2}O_2$ (NMC622) and b) NMCAT.

147.6 J g^{-1}. Furthermore, at 50% SOC, NMCAT revealed a peak at 274 °C with a Δ*H* value of 96.3 J g^{-1}, while the commercial NMC displayed a peak at 265 °C with a Δ*H* value of 140.3 J g^{-1}. Based on the above observations, it is evident that NMCAT (281 °C) exhibits superior thermal stability compared to pristine NMC622 (267 °C), which can be attributed to the inclusion of Al and Ti in the cathode formulation. This indicates that the layered architecture of NMCAT remains structurally stable, even when the cathode is fully depleted of Li. The enhanced stability is attributed to the higher bond dissociation energies of Al-O (512 ± 4 kJ mol^{-1}) and Ti-O (662 ± 16 kJ mol^{-1}) compared to Ni-O (391.6 ± 38 kJ mol^{-1}), Mn-O (402 ± 34 kJ mol^{-1}), and Co-O (368 ± 21 kJ mol^{-1}).[22]

The achieved results are worth to compare with some of the early reports. Noh et al. noticed the exothermicity of NMC622 at 260 °C with heat generation of 721.4 J g^{-1}.[13] Belharouak et al. studied the NMC111 cathode thermal stability and found decomposition at 260 °C with three more exothermic peaks and reported that the generated heat of NMC111 is 790 J g^{-1}.[23] Hiroaki et al. showed heat generation of NMC811 occurs in between 230–240 °C.[24]

2.3. Theoretical Validation

The experimental results are further validated using first-principles density functional theory (DFT) calculations of NMC622 and NMCAT compounds. A detailed description of the DFT methodologies is provided in the supporting information. The NMC622 structure and its atomic distribution are adopted from the LMO structure[25] and modified by substituting Al and Ti in the place of Co and Mn atoms, respectively.[21] The structure considered for the present work consists of six layers, where different cations were uniformly distributed to minimize the electrostatic repulsive interaction acting among them, and Li atoms are positioned between the layers as similar to typical cathode materials. The simulated cell (s.c.) comprises 96 atoms with the following composition (approximated value) for NMCAT compound: Ni (60%), Co (16%), Mn (16%), Ti (4%), and Al (4%). The optimized NMC622 and NMCAT structures are shown in Figure S7, Supporting Information. The lattice parameters of the former compound are observed to be $a = b = 5.74$ and $c = 28.08$ Å. After substituting Al and Ti, the structural parameters are compressed by 0.02 and 0.04 Å, respectively. The overall volume change of the NMCAT system is reduced by ≈7.5 $Å^3$. The formation energy (E_{FE}) of the NMCAT system is calculated from

$$E_{FE} = E(NMCAT) - E(NMC622) - \mu_s + \mu_r \quad (1)$$

where E(NMCAT) and E(NMC622) are the total energy of substituted and pristine systems, respectively, and the chemical potential of substituted and replaced atoms are denoted by μ_s and μ_a, respectively. The E_{FE} value is calculated to be −0.28 eV $s.c^{-1}$. The structural and energetic analyses confirm that the substitutions of Al and Ti atoms favor forming the stable structure. The experimental results demonstrate that the NMCAT compound exhibits superior thermal stability and cycling performance compared to the NMC622 compound. To investigate the underlying reasons for this enhanced thermal stability, DFT calculations were conducted on both NMC622 and NMCAT compounds with varying lithium concentrations (0%, 25%, 50%, 75%, and 100%). The atomic structures are presented in **Figure 3**, while the structural parameter variations are summarized in **Table 1**. Upon substituting Al and Ti atoms into the structure, slight variations in the lattice parameters along the *a* and *b* axes were observed, ranging from 0 to 0.09 Å, whereas a more significant change was noted in the *c*-axis lattice parameter. The volume contraction can be attributed to the substitution of smaller Al^{3+} ions and the introduction

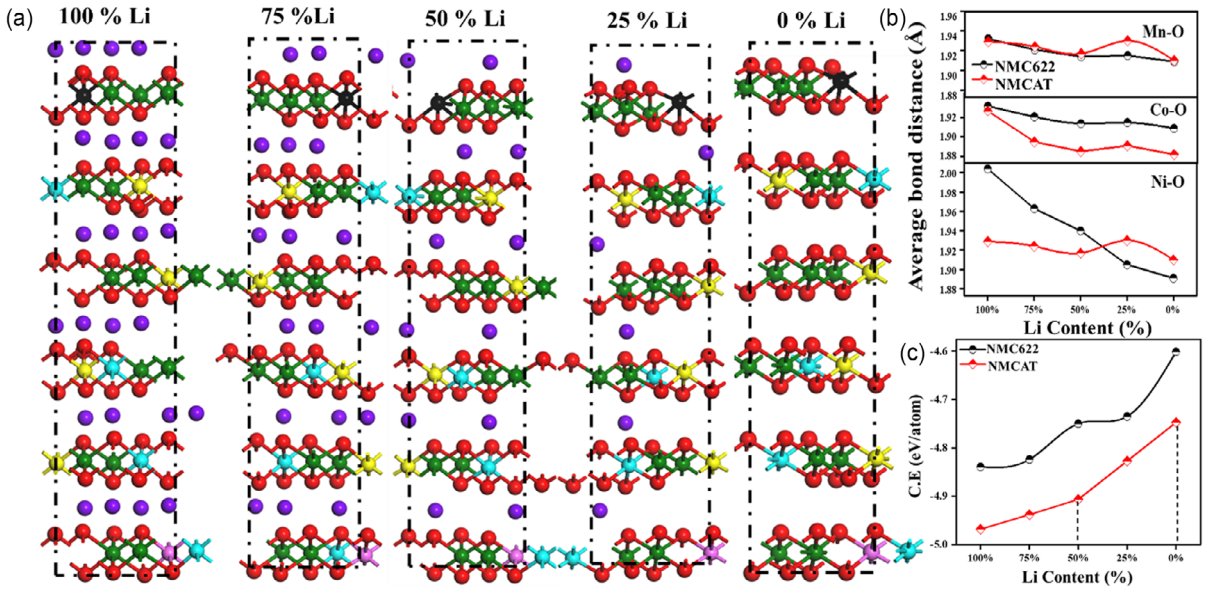

Figure 3. a) Ball and stick model of the NMCAT system with varying lithium contents. b) Average M—O bond distances. c) Cohesive energy (eV/atom) for lithiated NMC622 and NMCAT compounds. Green, cyan, yellow, red, magenta, black, and purple color balls represent Ni, Mn, Co, O, Al, Ti, and Li atoms, respectively.

Research Article
doi.org/10.1002/batt.202500320
Chemistry Europe
European Chemical Societies Publishing

Table 1. The volume change (ΔV) and variation in *c* lattice parameter (Δc) of NMCAT (as compared to NMC622) are given for various lithium contents.

Li content	ΔV [Å^3]	Δc [Å]
100%	7.5	0.04
75%	−0.83	−0.054
50%	−11.97	−0.967
25%	−7.75	−0.471
0%	−0.43	0.01

of Ti^{4+} ions, which contribute an additional electron, thereby facilitating stronger bonding within the NMCAT structure. To evaluate bonding strength, cohesive energy (E_{CE}) is typically calculated by subtracting the total energy of the compound from the sum of the atomic energies of its constituent atoms. The E_{CE} values for NMC622 and NMCAT with varying lithium contents are shown in Figure 3c. The results indicate that the E_{CE} for NMCAT is significantly higher than that of NMC622, suggesting enhanced structural stability due to the presence of Al^{3+} and Ti^{4+} ions.

The structural stability of both cathode materials during cycling processes was also assessed. For NMC622, a noticeable shoulder at 50% lithium content highlights instability in the system. This sharp variation in E_{CE}, particularly as lithium concentration decreases from 75 to 50%, is likely released as heat energy, contributing to thermal runaway in NMC622, as observed experimentally. In contrast, such variations are largely suppressed in the NMCAT compound, allowing it to maintain structural stability during charging and discharging cycles.

The incorporation of Ti^{4+} and Al^{3+} substituents in the NMC622 structure not only enhances its structural stability but also minimizes significant energy profile fluctuations, thereby improving its performance under cycling conditions.

To gain atomic-level insights further, the M—O bond distances in NMC622 and NMCAT compounds were analyzed across various lithium contents, as shown in Figure 3b. The average Mn—O bond distances in both compounds exhibit minimal variation, except at 25% lithium content, indicating that the MnO_6 octahedral structure remains largely intact even with the substitution of Al and Ti atoms. In contrast, significant changes are observed in the Ni—O and Co—O bond distances, attributed to the involvement of an additional electron. Notably, the Ni—O bond distances vary considerably between the two compounds across different lithium contents. In NMC622, a substantial reduction in Ni—O bond distance occurs during delithiation, whereas in NMCAT, this bond distance remains nearly constant. This stability in Ni—O bond distance confirms the superior structural robustness of the NMCAT compound during charging and discharging cycles, enabling it to withstand thermal runaway more effectively than NMC622.

Electronic properties are also deduced for NMC622 and NMCAT compounds with various lithium contents to investigate the electronic contributions towards their structural stability and electrochemical properties. **Figure 4** and S8, Supporting Information, presents the density of states (DOS) and partial density of state (PDOS) demonstrating the enhanced structural stability of the modified system compared to the formed system. This is evident from the pronounced energy level splitting between the occupied (Co-3 d-t_{2g}) and unoccupied (Co-3 d-e_g) states. It is also noted that

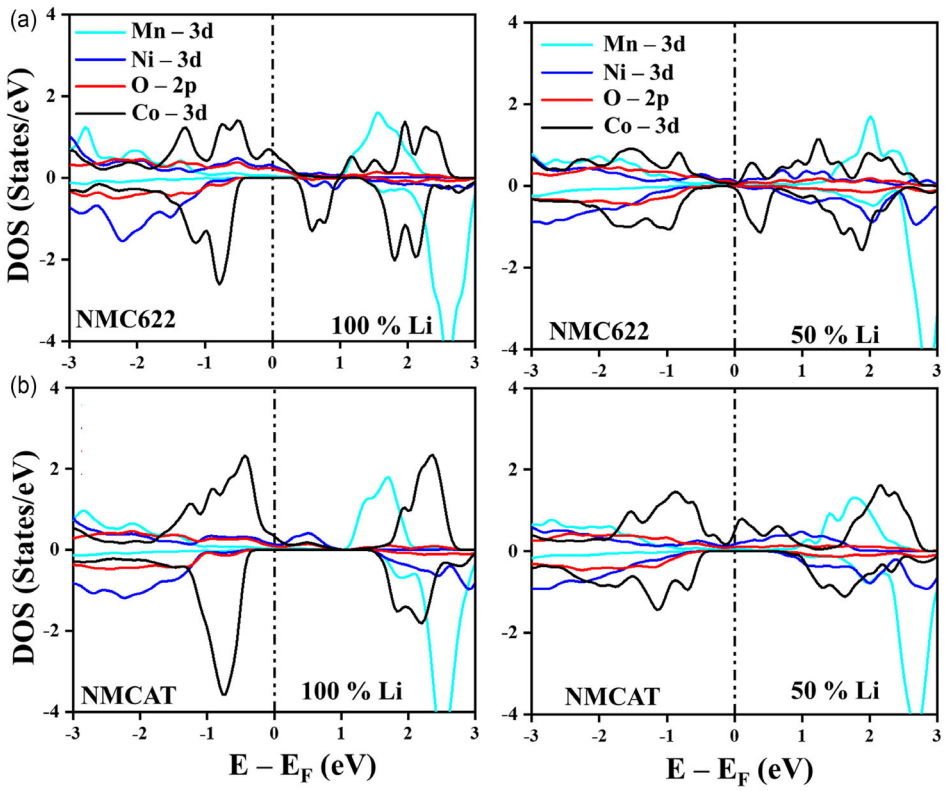

Figure 4. PDOS for the system with 100% and 50% Li content of NMC622 (top panels) and NMCAT (bottom panels).

Ni-3 d states around the Fermi energy (E_F) are well dispersed owing to its higher atomic concentration in those compounds, while Mn-3 d states are well apart from E_F level, indicating the electrochemical inactiveness of Mn atoms, in addition to Al^{3+} and Ti^{4+} ions, during the cycling processes. Almost similar trend in DOSs is also observed for 50% lithiated cases of both compounds. Overall, during the cycling process of the NMCAT compound, Co and Ni atoms are only involved in oxidation and reduction processes. The distribution of *O*-2p levels in both compounds is also deduced, and the results are shown in Figure S9, Supporting Information. It indicates that the width of the *O*-2p level in NMCAT is higher as compared to that level in NMC622, revealing the strong *p*-d hybridization between *M*-3 d and *O*-2p states owing to the shorter M—O distances. Overall, our DFT calculations showed that NMCAT compound exhibits superior thermal stability during 50% lithiation due to the following factors: (i) the substitution of Ti and Al atomic improves structural stability of the compound, (ii) the contraction in volume enhances the hybridization between *O*-2p and *M*-3 d states, and (iii) Ni and Co are only participated in electrochemical processes.

3. Conclusions

A thermally stable Ni-rich cathode material, $LiNi_{0.6}Mn_{0.15}Co_{0.15}Al_{0.05}Ti_{0.05}O_2$, was developed and extensively characterized in terms of its structural, electrochemical, and thermal properties. The structural analysis confirmed that the composition possesses a layered structure with an ABCABC stacking arrangement. The inclusion of Al and Ti in the composition provides structural support, ensuring the stability of the layered structure even under full charge conditions. Thermal investigations using calorimetry demonstrated that the prepared material exhibits excellent thermal stability, with no significant exothermic reactions observed up to a temperature of 280 °C. Notably, the presented composition exhibited the lowest exothermicity ($\Delta H = 175.6\ J\ g^{-1}$) among the reported materials and commercially available NMC622, indicating its enhanced thermal safety. Further, the DFT analysis validated experimental results that the substitution of Al^{3+} and Ti^{4+} in NMC622 to form NMCAT significantly enhances structural stability. The higher cohesive energy in NMCAT indicates stronger bonding, while the stability of Ni—O bond distances across varying lithium contents confirms its robustness during cycling. These improvements mitigate drastic energy variations and reduce the risk of thermal runaway, making NMCAT a more reliable cathode material for practical applications. The combination of structural and thermal stability makes $LiNi_{0.6}Mn_{0.15}Co_{0.15}Al_{0.05}Ti_{0.05}O_2$ a highly attractive material for energy storage applications, particularly in the context of battery safety. The choice of cathode material is crucial in mitigating the risk of thermal runaway, which is influenced by various factors, including the cathode, electrolyte, and mechanical/electrical abuses. In this regard, the unique composition $LiNi_{0.6}Mn_{0.15}Co_{0.15}Al_{0.05}Ti_{0.05}O_2$ emerges as a promising candidate to address the issue of thermal runaway from a cathode material standpoint. Hence, by using this cathode material, the risk of thermal runaway can be significantly reduced.

Acknowledgements

The authors thank DST-AMEST (Project No: GAP 10/24) for the financial support.

Conflict of Interest

The authors declare no conflict of interest.

Data Availability Statement

The data that support the findings of this study are available from the corresponding author upon reasonable request.

Keywords: cathode · differential scanning calorimetry · doping · Li-ion battery · NMC622 · SEM · thermal stability

[1] Z. Tang, D. Feng, Y. Xu, L. Chen, X. Zhang, Q. Ma, *Batteries* **2023**, *9*, 156.
[2] L. De Biasi, B. Schwarz, T. Brezesinski, P. Hartmann, J. Janek, H. Ehrenberg, *Adv. Mater.* **2019**, *31*, 1900985.
[3] X. Feng, M. Ouyang, X. Liu, L. Lu, Y. Xia, X. He, *Energy Storage Mater.* **2018**, *10*, 246.
[4] D. D. Macneil, L. Christensen, J. Landucci, J. M. Paulsen, J. R. Dahn, *J. Electrochem. Soc.* **2000**, *147*, 970.
[5] Y. Sun, D. Ren, G. Liu, D. Mu, L. Wang, B. Wu, J. Liu, N. Wu, X. He, *Int J Energy Res.* **2021**, *45*, 20867.
[6] K. Liu, Y. Liu, D. Lin, A. Pei, Y. Cui, *Sci. Adv.* **2018**, *4*, 1.
[7] S. M. Bak, E. Hu, Y. Zhou, X. Yu, S. D. Senanayake, S. J. Cho, K. B. Kim, K. Y. Chung, X. Q. Yang, K. W. Nam, *ACS Appl. Mater. Interfaces* **2014**, *6*, 22594.
[8] J. Guo, Y. Li, J. Meng, K. Pedersen, L. Gurevich, D. I. Stroe, *J. Energy Chem.* **2022**, *74*, 34.
[9] A. K. Budumuru, V. Hebbar, M. Viji, C. Sudakar, *Mater. Lett.: X* **2021**, *11*, 100089.
[10] R. Tatara, Y. Yu, P. Karayaylali, A. K. Chan, Y. Zhang, R. Jung, F. Maglia, L. Giordano, Y. Shao-Horn, *ACS Appl. Mater. Interfaces* **2019**, *11*, 34973.
[11] X. Lu, N. Zhang, M. Jahn, W. Pfleging, H. J. Seifert, *Appl. Sci.* **2019**, *9*, 3671.
[12] T. T. D. Nguyen, S. Abada, A. Lecocq, J. Bernard, M. Petit, G. Marlair, S. Grugeon, S. Laruelle, *World Electr. Veh. J.* **2019**, *10*, 79.
[13] H. J. Noh, S. Youn, C. S. Yoon, Y. K. Sun, *J Power Sources* **2013**, *233*, 121.
[14] X. Feng, S. Zheng, X. He, L. Wang, Y. Wang, D. Ren, M. Ouyang, *Front. Energy Res.* **2018**, *6*, 1.
[15] G. Guihong, Z. Liming, Y. Jieyu, Y. Tengyu, X. Fangming, T. Renheng, S. Xin, W. Ying, S. Laifa, *J. Mater. Chem. A* **2024**, *12*, 12645.
[16] Y. Jieyu, M. Guihong, Y. Tengyu, S. Laifa, Y. Yan, *Angew. Chem. Int. Ed.* **2025**, *64*, e202420413.
[17] K. Momma, F. Izumi, *J. Appl. Crystallogr.* **2011**, *44*, 1272.
[18] T. Wang, H. Luo, J. Fan, B. P. Thapaliya, Y. Bai, I. Belharouak, S. Dai, *iScience* **2022**, *25*, 1.
[19] Y. K. Sun, D. J. Lee, Y. J. Lee, Z. Chen, S. T. Myung, *ACS Appl. Mater. Interfaces* **2013**, *5*, 11434.
[20] J. Dahn, W. Fuller, *Solid State Ionics* **1994**, *69*, 265.
[21] F. Baakes, M. Luthe, M. Gerasimov, V. Laue, F. Roder, P. Balbuena, U. Krewer, *J. Power Sources* **2022**, *522*, 230881.
[22] J. A. Dean, A. John, N. A. Lange, *Lange's Handbook of Chemistry*, McGraw-Hill, USA **1999**.
[23] I. Belharouak, W. Lu, D. Vissers, K. Amine, *Electrochem. Commun.* **2006**, *8*, 329.
[24] K. Hiroaki, Y. Masanori, H. Tatsumi, *J. Power Sources* **2013**, *244*, 23.
[25] G. Cerder, V. Anton, *Electrochim. Acta* **1999**, *45*, 131.

Manuscript received: April 28, 2025
Revised manuscript received: June 13, 2025
Version of record online: